NANO LETTERS
Cite This: Nano Lett. XXXX, XXX, XXX−XXX
Letter
pubs.acs.org/NanoLett

A Direct Comparison of in Vitro and in Vivo Nucleic Acid Delivery Mediated by Hundreds of Nanoparticles Reveals a Weak Correlation

Kalina Paunovska,[†,⊥] Cory D. Sago,[†,⊥] Christopher M. Monaco,[†,‡] William H. Hudson,[§] Marielena Gamboa Castro,[†] Tobi G. Rudoltz,[†] Sujay Kalathoor,[†] Daryll A. Vanover,[†] Philip J. Santangelo,[†] Rafi Ahmed,[§] Anton V. Bryksin,[∥] and James E. Dahlman*[,†]

[†]Wallace H. Coulter Department of Biomedical Engineering, Georgia Institute of Technology and Emory University School of Medicine, Atlanta, Georgia 30332, United States

[‡]School of Biological Sciences, Georgia Institute of Technology, Atlanta, Georgia 30332, United States

[§]Emory Vaccine Center and Department of Microbiology and Immunology, Emory University School of Medicine, Atlanta, Georgia 30317, United States

[∥]Parker H. Petit Institute for Bioengineering and Bioscience, Georgia Institute of Technology, Atlanta, Georgia 30332, United States

Supporting Information

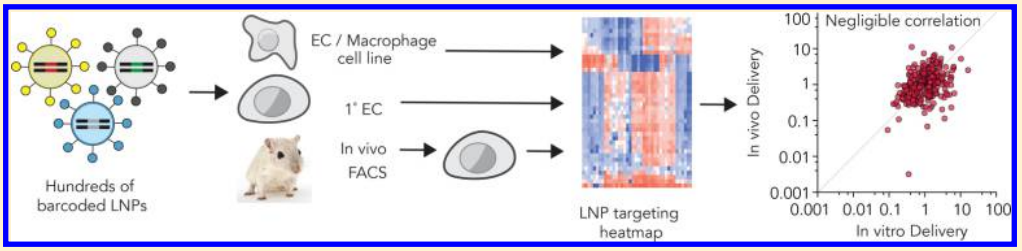

ABSTRACT: Endothelial cells and macrophages play active roles in disease and as a result are important targets for nucleic acid therapies. While thousands of chemically distinct lipid nanoparticles (LNPs) can be synthesized to deliver nucleic acids, studying more than a few LNPs in vivo is challenging. As a result, it is difficult to understand how nanoparticles target these cells in vivo. Using high throughput LNP barcoding, we quantified how well LNPs delivered DNA barcodes to endothelial cells and macrophages in vitro, as well as endothelial cells and macrophages isolated from the lung, heart, and bone marrow in vivo. We focused on two fundamental questions in drug delivery. First, does in vitro LNP delivery predict in vivo LNP delivery? By comparing how 281 LNPs delivered barcodes to endothelial cells and macrophages in vitro and in vivo, we found in vitro delivery did not predict in vivo delivery. Second, does LNP delivery change within the microenvironment of a tissue? We quantified how 85 LNPs delivered barcodes to eight splenic cell populations, and found that cell types derived from myeloid progenitors tended to be targeted by similar LNPs, relative to cell types derived from lymphoid progenitors. These data demonstrate that barcoded LNPs can elucidate fundamental questions about in vivo nanoparticle delivery.

KEYWORDS: *DNA barcoded nanoparticles, nanotechnology, drug delivery, siRNA, gene editing*

The transport of foreign nucleic acids is carefully regulated, making systemic drug delivery inefficient.[1−3] To deliver nucleic acids, thousands of chemically distinct lipid nanoparticles (LNPs) have been designed.[4−9] LNP chemical diversity is imparted two ways. First, thousands of distinct biomaterials have been synthesized.[4−9] Second, each biomaterial can be formulated into hundreds of LNPs by adding poly(ethylene glycol) (PEG), cholesterol, 1,2-dioleoyl-*sn*-glycero-3-phosphoethanolamine (DOPE), and other constituents at different mole ratios. LNPs are screened in vitro before a small number of finalists is tested in vivo;[4−9] in a typical example, we measured how well 2,000 LNPs delivered siRNA to HeLa cells in static cell culture before analyzing 5 LNPs in vivo.[5] Similar studies have been performed with LNPs composed of small amine-, sugar-, or peptide-based materials.[4,6−9]

To successfully deliver nucleic acids after systemic administration, nanoparticles must overcome complex obstacles that are difficult to model in vitro. A significant fraction of the drug can be lost at each point and, as a result, every step is important to model. For example, cationic nanoparticles can be disassembled by the renal anionic basement membrane,[10] and nanoparticles can be blocked from accessing brain parenchyma due to the capillary tight junctions and glial cells that make up the blood brain barrier.[11−15] By contrast, nanoparticles can access tissues like the liver via porous ECs and discontinuous basement membranes in the hepatic sinusoids.[11−15] In addition

Received: January 30, 2018
Revised: February 25, 2018
Published: February 28, 2018

DOI: 10.1021/acs.nanolett.8b00432
Nano Lett. XXXX, XXX, XXX−XXX

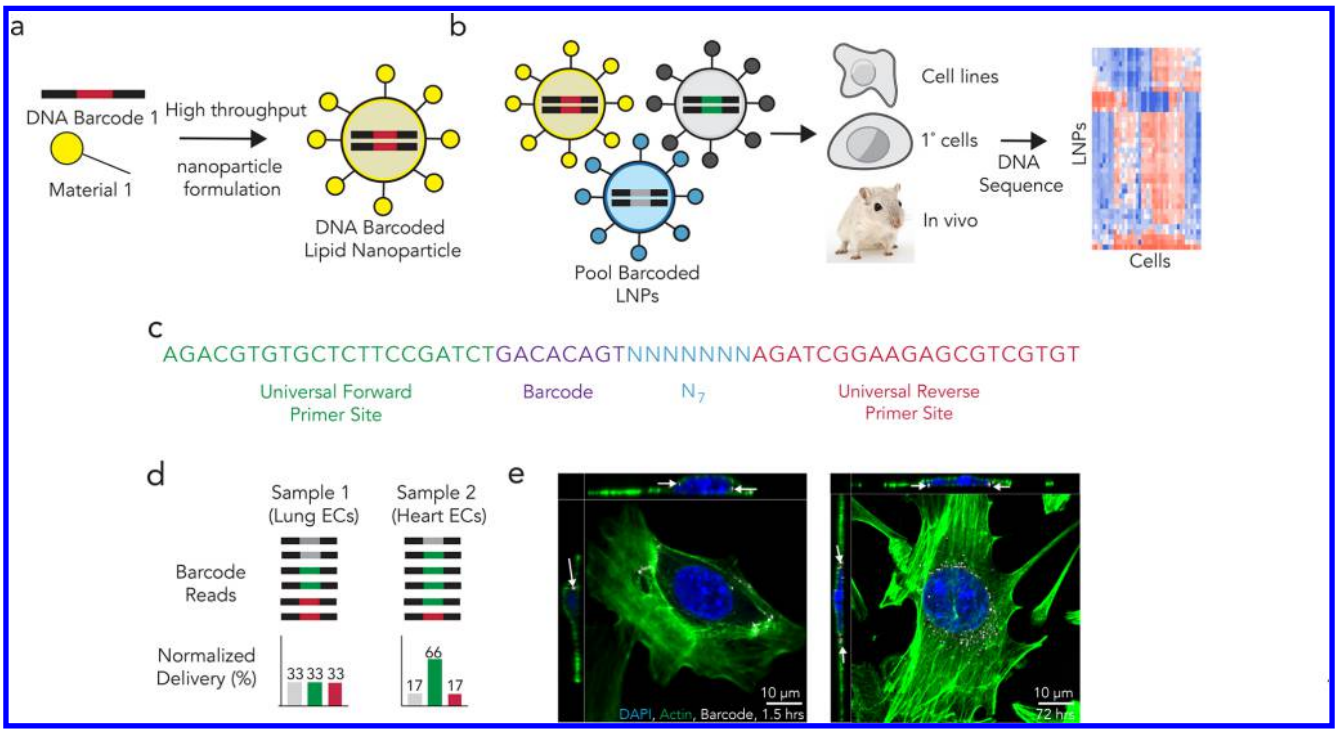

Figure 1. JORDAN, a system for high throughput in vivo nanoparticle analysis. (a) Lipid nanoparticles (LNPs) were formulated to carry DNA barcodes, before (b) stable LNPs were pooled together and administered to cells or mice. Cells were deep sequenced to quantify the relative delivery of all the LNPs simultaneously. (c) The DNA barcode was rationally designed with universal primer sites and a randomized seven nucleotide region to minimize PCR bias. (d) Normalized delivery for every barcoded LNP was calculated. In this example schematic, all three barcodes were equally represented in Sample 1, while in Sample 2, the green barcode was overrepresented. We would hypothesize that the gray LNP delivered DNA more efficiently to Sample 2 than the yellow or blue LNP. The full data analysis to calculate normalized delivery is described in Figure S1c. (e) Alexa-647 fluorescence 1.5 and 72 h after cells were transfected with 20 ng of Alexa Fluor 647 tagged DNA barcode formulated into the LNP 7C1.

to these barriers, blood flow rates affect nanoparticle targeting by affecting the likelihood a particle leaves the bloodstream.[16]

Despite these differences, nanoparticles are often screened in vitro. Large scale in vitro nanoparticle screens typically utilize cells that are easy to expand (e.g., HeLa).[4−9] These cells have genotypes and phenotypes that differ from cells in vivo. Cells can also undergo significant changes in gene expression when cultured.[17] Many of these changes may be driven by exposure to a combination of foreign serum (e.g., FBS) and static fluid flow, which most cell types are not exposed to in vivo. Given that in vitro and in vivo delivery require the nanoparticle to overcome different physiological obstacles and that endocytosis is likely to be affected by gene expression changes that occur when cells are removed from their natural microenvironment, we hypothesized that in vivo LNP delivery would not be predicted in vitro using common cell culture conditions.

The field can currently synthesize nanomaterials at a rate several orders of magnitude higher than the rate at which we can test nanomaterials for drug delivery in vivo. Recently, we reported a nanoparticle DNA barcoding system[18] to increase the number of LNPs we could study at once in vivo. We used a microfluidic device to barcode LNPs (Figure 1a);[19] each LNP was formulated to carry a unique DNA barcode. We pooled stable LNPs, administered them to animals, and deep sequenced the barcodes to quantify the delivery of up to 30 LNPs simultaneously.[18] This original paper focused exclusively on control experiments designed to characterize the system. Specifically, we demonstrated that barcoded LNPs can be made so they do not mix in solution, that DNA sequencing readouts were linear with respect to the amount of injected DNA, that DNA barcode delivery recapitulates the behavior of previously characterized LNPs, that delivery does not change with DNA sequence, and that delivery of DNA barcodes to hepatocytes in vivo modeled siRNA delivery to hepatocytes in vivo.[18]

We now report that the same LNP barcoding system, herein named JOint Rapid DNA Analysis of Nanoparticles (JORDAN), can elucidate fundamental questions about nanoparticle delivery. We quantified how well 281 LNPs delivered DNA barcodes to endothelial cells and macrophages, both in vitro and in vivo. We focused on endothelial cells and macrophages for three reasons. First, both cell types are implicated in many diseases.[20,21] Second, because they are ubiquitous we could measure delivery to the same cell type in multiple tissues. Third, endothelial cells are more "accessible" upon intravenous injection than tissue macrophages. We reasoned, incorrectly, that delivery to more accessible cells would be more predictable in vitro. Our data strongly suggest that in vitro LNP delivery to endothelial cells and macrophages using static cell culture does not predict in vivo LNP delivery to the same cell types.

We then used the JORDAN system to investigate how different LNPs distribute within the spleen, an important clearance organ. By measuring how 85 LNPs delivered barcodes to 8 different splenic cell types, we found that cells derived from myeloid progenitors tended to be targeted to by similar LNPs; cells derived from lymphoid progenitors tended to be targeted by different LNPs. We then identified LNP1, which delivered barcodes to all eight cell types we studied in the spleen. We confirmed the splenic targeting of LNP1 using fluorescently labeled DNA. The approach we have described can be extended to study (i) how well any in vitro system (e.g.,

DOI: 10.1021/acs.nanolett.8b00432
Nano Lett. XXXX, XXX, XXX−XXX

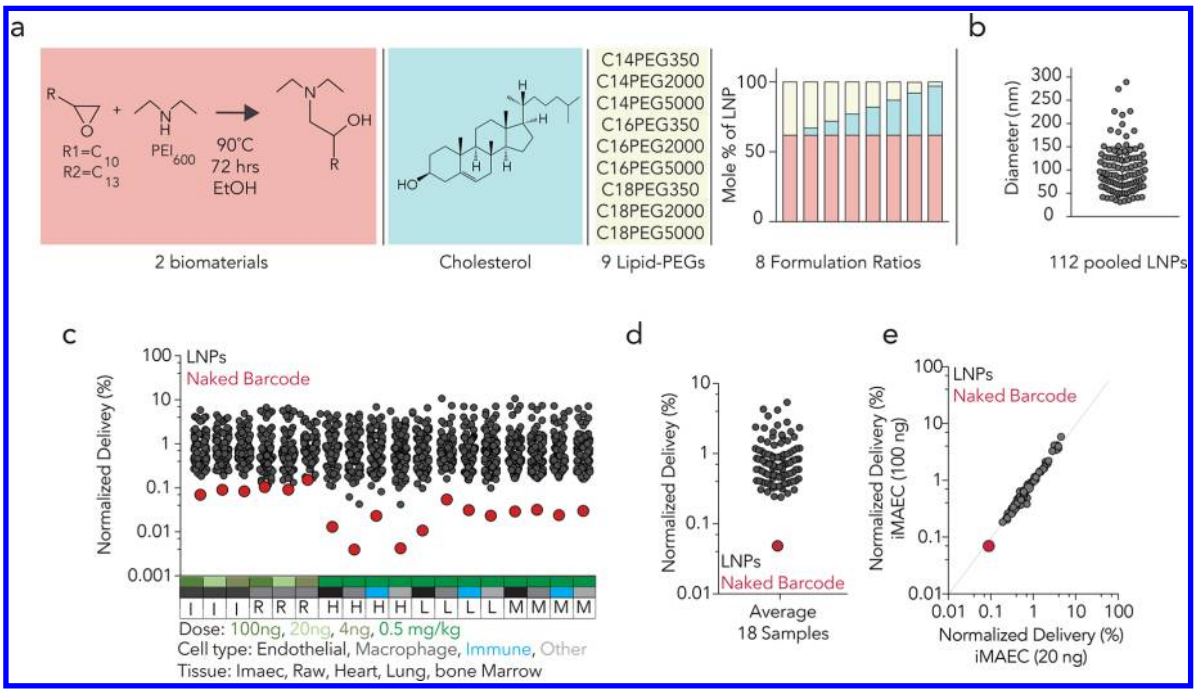

Figure 2. To analyze the robustness of our system, (a) we formulated 144 chemically distinct LNPs, (b) pooled stable LNPs and administered them to two cell lines (RAWs, iMAECs) and mice. (c) Normalized delivery for all LNPs and naked barcode in 18 cell and tissue types. (d) Average normalized delivery for all 18 samples. The naked barcode delivered DNA less efficiently than all LNPs. (e) Normalized delivery in iMAECs 72 h after 20 or 100 ng total DNA was administered. In vitro delivery to iMAECs at 20 ng/well predicted in vitro delivery to iMAECs at 100 ng/well.

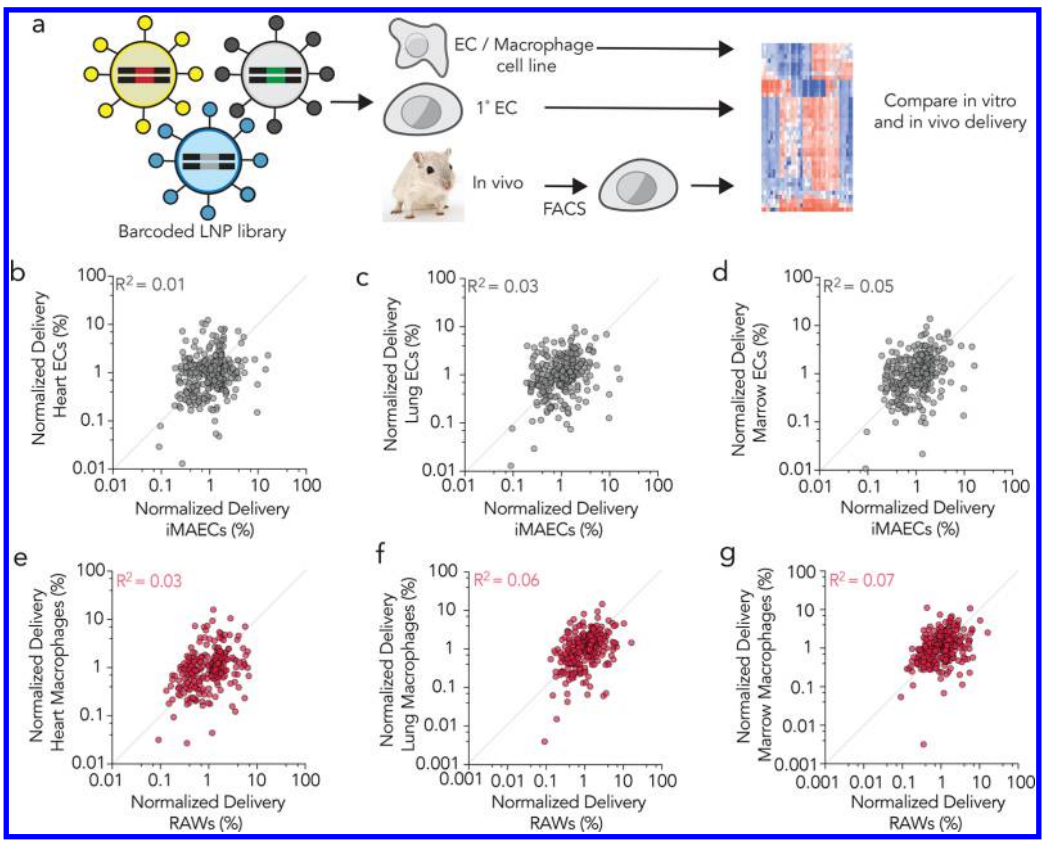

Figure 3. A direct comparison between in vitro and in vivo nanoparticle delivery. (a) LNPs (420) were formulated and delivery was compared between in vivo FACS sorted cells, primary cells, and cell lines. (b–d) Normalized delivery of LNPs in iMAECs and heart, lung, and bone marrow endothelial cells. (e–g) Normalized delivery of LNPs in RAWs and heart, lung, and bone marrow macrophages. In both cases, in vitro LNP delivery does not predict in vivo delivery.

DOI: 10.1021/acs.nanolett.8b00432
Nano Lett. XXXX, XXX, XXX−XXX

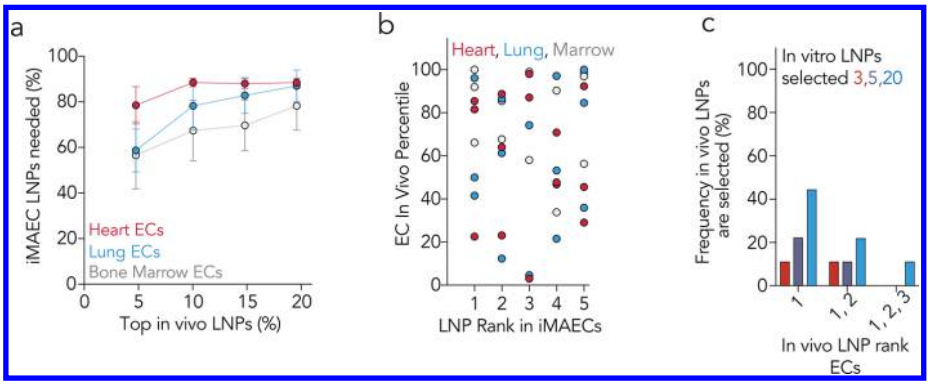

Figure 4. Quantifying the efficiency with which in vitro screens predict in vivo delivery. (a) Percentage of in vitro LNPs required to encompass the top 5, 10, 15, and 20% of the LNPs in heart, lung, and bone marrow endothelial cells in vivo. For example, over 50% of the in vitro library would be required to ensure the top 5% of the in vivo LNPs were selected. (b) LNP rank in vivo in heart, lung, and bone marrow endothelial cells for the top five in vitro ranked LNPs. (c) Frequency with which the first, first and second, or first, second, and third in vivo LNPs would be chosen by selecting the top 3, 5, and 20 LNPs in vitro.

tissue-on-a-chip) predicts delivery in vivo and (ii) how different cells are targeted within a tissue.

Results. We rationally designed DNA barcodes in order to study the delivery of many LNPs at once (Figure 1a–c). Each DNA barcode contained phosphorothioate linkages in order to reduce exonuclease activity, and universal primer sites for unbiased polymerase chain reaction (PCR) amplification (Figure 1c).[18] The 8 nucleotide "barcode" region was located in the middle of the 56 nucleotide DNA sequence. Of the 4^8 possible DNA barcode combinations, we designed 240 to work with Illumina sequencing machines (Figure S1a). We amplified barcodes using universal primers and labeled individual samples with Illumina dual-indexed adapters that enabled sample multiplexing (Figure S1b). For each experiment, we calculated the "normalized delivery", using the administered LNP solution as a DNA input (Figure 1d, Figure S1c). We also added new LNP quality controls to reduce the likelihood of LNPs mixed together. Specifically, we analyzed the size of each individual LNP using dynamic light scattering (DLS). On the basis of our experience studying LNPs,[5,18,22−25] we only pooled stable LNPs with good autocorrelation curves and diameters between 20 and 300 nm (Figure S1d). We then tested whether barcoded LNPs entered cells. We formulated Alexa647-tagged DNA barcodes in a previously characterized[5,18,22−27] LNP named 7C1. Barcodes entered immortalized mouse aortic endothelial cells (iMAECs) within 15 min and were observed inside the cell at 1.5 and 72 h after administration (Figure 1e, Figure S1e,f).

We then formulated a library of 144 LNPs, library 1, systematically varying PEG structure. We synthesized two biomaterials called "lipomers", which are lipid-amines conjugates created by reacting epoxide, acrylate, or methacrylate-terminated lipids with oligoamines.[5,7,18,28,29] Both lipomers were formulated into 72 LNPs, using 9 different PEGs and 8 different PEG mole percentages, for a total of 144 LNPs (Figure 2a, Figure S2a). One hundred and twelve out of 144 formulations formed stable LNPs and were pooled (Figure 2b). We administered the 112 stable LNPs, as well as a naked DNA barcode, which served as a negative control, to cells at a total DNA dose of 4, 20, and 100 ng/well, in a 24 well plate. Concurrently, we administered the LNPs to mice via a tail vein injection at a total dose of 0.5 mg/kg DNA. We isolated DNA from cells or tissues 72 h later, a time point we chose to minimize the influence of dynamic endocytic processes.[5,30−33] The 4 ng total DNA dose equaled an average DNA dose of 0.035 ng/well/LNP, demonstrating the sensitivity of the DNA barcoding system. We administered the LNPs to immortalized mouse aortic endothelial cells (iMAECs) and mouse macrophages (RAWs). We chose iMAECs because they are isolated directly from the murine heart and have been shown to recapitulate endothelial cell signaling and function.[34] We chose RAWs because they are a commonly used macrophage cell line.

We examined positive and negative controls to evaluate whether this data set was robust. The naked barcode (negative control) performed poorly compared to LNP-delivered DNA in all 18 samples (Figure 2c,d). LNP delivery in iMAECs and RAWs treated with 20 ng total DNA predicted LNP delivery in iMAECs and RAWs treated with 4 or 100 ng DNA with high precision ($R^2 > 0.9$) (Figure 2e, Figure S2b–d). Put another way, in this positive control experiment delivery to iMAECs in vitro at one dose predicted delivery to iMAECs at two other doses.

We then investigated whether in vitro LNP delivery predicted in vivo LNP delivery (Figure 3a). We compared normalized delivery in iMAECs and RAWs to endothelial cells (ECs) and macrophages isolated from mice injected with LNPs. We isolated endothelial cells and macrophages from mice using a fluorescence activated cell sorting (FACS) protocol we previously established[5,18,22,26] (Figure S3a–c). In vitro iMAEC delivery did not predict in vivo delivery to heart, lung, or bone marrow endothelial cells (Figure S3j–l). Similarly, delivery to RAWs in vitro did not predict delivery to heart, lung, or bone marrow macrophages (Figure S3s–u). To validate these results, we synthesized two additional LNP libraries. Library two consisted of 120 LNPs of which 105 were found to be stable by DLS and included (Figure S3d,e). In this library, we systematically varied the lipid tail and amine reacted to make the lipomer component of each LNP. Library three consisted of 156 LNPs of which 64 were found to be stable by DLS and included (Figure S3f,g). In this library, we systematically varied the PEG tail length and molecular weight (MW), using three different tail lengths (C14, C16, C18) and two different MWs (350, 2000 Da). Results from libraries two and three recapitulated results from library one; in vitro delivery to endothelial cells and macrophages did not predict in vivo delivery to the same cell types. In total, we performed three experiments, formulating 420 LNPs of which 281 were stable and included (Figure S3h,i). Results from each individual

DOI: 10.1021/acs.nanolett.8b00432
Nano Lett. XXXX, XXX, XXX−XXX

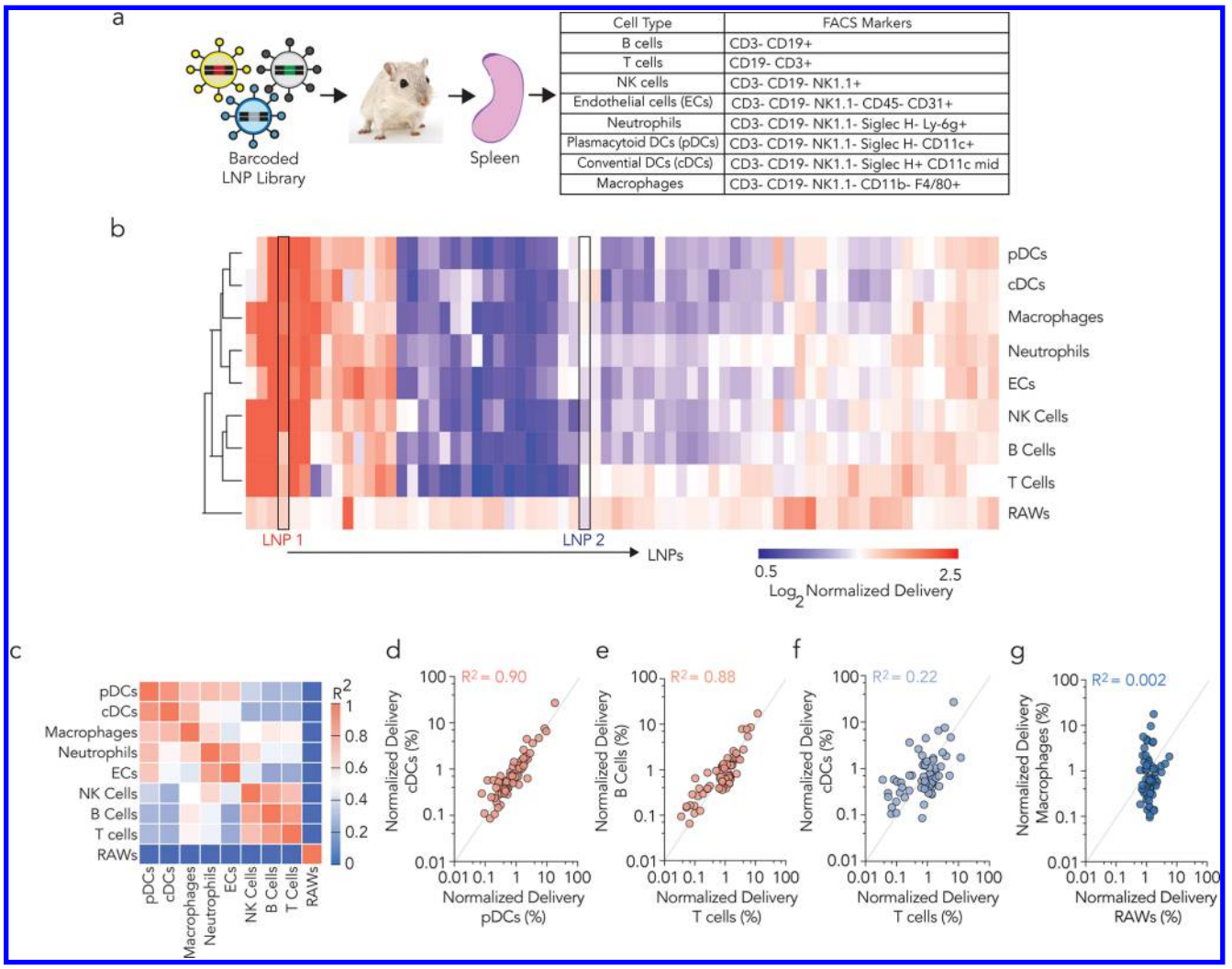

Figure 5. High-throughput analysis of delivery to splenic microenvironment. (a) LNPs (144) were formulated; 85 stable LNPs were pooled and administered to WT mice. Seventy-two hours later, cell types were isolated from the spleen using FACS. (b) Unbiased clustering of LNPs in each cell type, generated by a Euclidean distance algorithm. RAWs (macrophage in vitro) clustered separately from all 8 in vivo cell types, and both dendritic cell populations clustered together. (c) R^2 values for all eight in vivo cell types as well as RAWs. Normalized delivery in (d) plasmacytoid and conventional dendritic cells (DCs), (e) B cells and T cells, (f) conventional DCs and T cells, and (g) RAWs and splenic macrophages.

experiment are plotted in Figure S3j–aa. Combined results from all three experiments are plotted in Figure 3b–g.

We considered the possibility that our results were due to a poor choice of cell line or time-point. To exclude this possibility, we investigated to what extent the (i) cell line and (ii) experimental time point altered the predictivity of in vitro delivery. We performed these experiments using library two. We administered library two to iMAECs, RAWs, and mice, and measured delivery 4, 48, and 72 h after LNP administration (Figure S3m–o,v–x,bb–ll). At all three time points, we also measured LNP delivery to the following three primary human endothelial cell lines: human aortic endothelial cells (HAECs), human aortic vein endothelial cells (HAVECs), and human umbilical vein endothelial cells (HUVECs). In all cases, we observed no strong relationship between in vitro and in vivo delivery (Figure S3mm–uu).

We then analyzed our data set with the goal of quantifying the "efficiency" of traditional in vitro screening. Put another way, if a LNP library is screened in vitro and a small number of LNPs is selected for in vivo analysis, how likely is it that the best in vivo candidate is selected? We first calculated the percentage of an in vitro library required to select the top 5, 10, 15, or 20% of in vivo LNPs. To ensure the top 5% of in vivo LNPs were selected, more than 50% of the in vitro library would need to be selected (Figure 4a, Figure S4a). We then analyzed how well the best in vivo LNPs performed in vitro. We ranked LNPs based on their in vitro performance. We then colored the LNPs that performed in the top 10% in vivo and listed their respective LNP compositions and sizes (Figure S4d–g). Some LNPs that performed well in vivo also performed well in vitro. However, in many cases LNPs that performed well in vivo did not rank highly in vitro; these LNPs would likely be discarded after an in vitro screen. Third, we evaluated how the top in vitro LNPs performed in vivo. Top ranked in vitro LNPs did not consistently perform well in vivo (Figure 4b, Figure S4b). More specifically, we plotted the in vivo rank (Y-axis) for each of the top five in vitro LNPs and found that the top five in vitro LNPs often performed poorly in vivo. This result was consistent for three in vivo endothelial beds (Figure 4b), as well in vivo macrophages from three tissues (Figure S4b). On the basis of this result, we asked a fourth question: if we selected the top 3, 5, or 20 in vitro LNPs,

DOI: 10.1021/acs.nanolett.8b00432
Nano Lett. XXXX, XXX, XXX–XXX

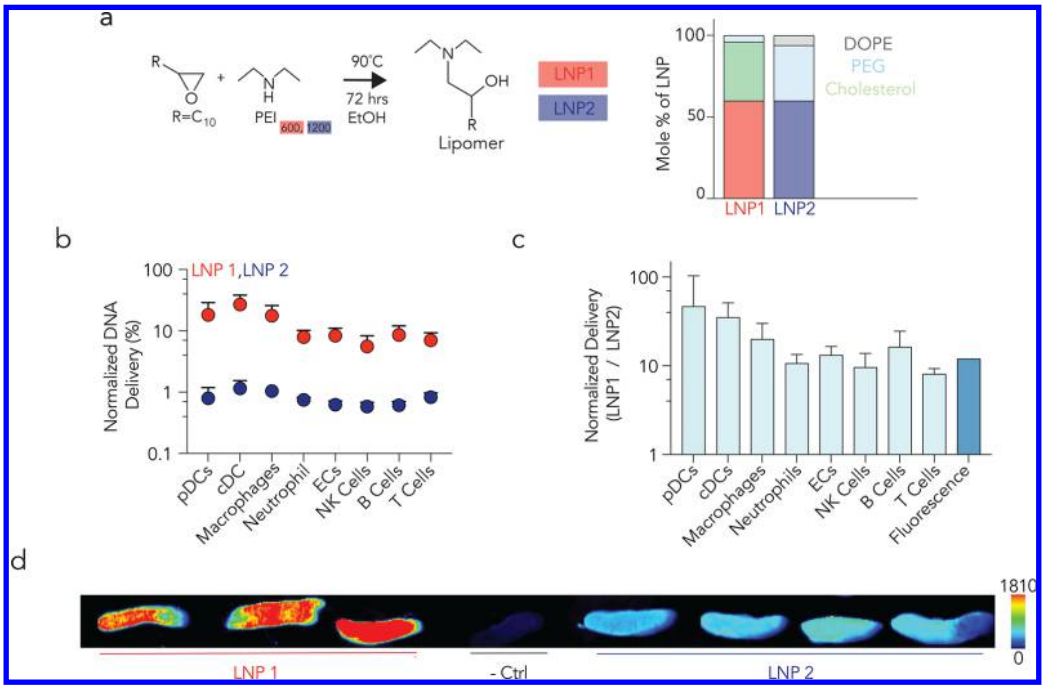

Figure 6. (a) Chemical compositions of LNP1 and LNP2. (b) Normalized delivery of two LNPs, one with high (LNP1) and one with low (LNP2) normalized delivery. (c) The ratio of normalized delivery (LNP1/LNP2) in each cell type using barcodes, as well as fluorescence of the spleen whole tissue. (d) Cy5.5 fluorescence in splenic whole tissue 3 h after mice were injected with either LNP1 or LNP2. LNP1 fluorescence was higher, as predicted by the barcoding data.

how likely were we to pick the first, first and second, or first, second, and third ranked in vivo LNPs? The odds of finding the top LNP for 3 in vivo endothelial cell beds were 11%, 22%, and 44% using the top 3, 5, and 20 in vitro LNPs, respectively; the odds of finding the top 2, or top 3 in vivo LNPs were lower (Figure 4c). We performed the same analyses for in vivo macrophages from three tissues and obtained similar results (Figure S4c). Taken together, these data strongly that in vitro delivery may not predict systemic in vivo delivery. While they do not directly implicate all in vitro systems or all cell types, they do strongly suggest each in vitro system should be validated using many nanoparticles before being used as the basis for nanoparticle discovery.

The JORDAN system generates large nanoparticle data sets; the size of these data sets enabled us to analyze the relationship between LNP properties and in vivo delivery. We plotted DNA barcode delivery as a function of each material property. In total, we analyzed 309 relationships between LNP structure and in vivo delivery. We found that the lipomer alkyl tail length, lipomer amine structure, and PEG molecular weight were most likely to influence LNP delivery (Figure S4h). These results suggest that the structure of the amine-lipid compound as well as the structure of PEG both strongly influence LNP targeting. These results provide an important insight into LNP library design and substantiate previously reported nanoparticle research.[35−37] One important limitation is that we were not able to identify a mathematical framework with assumptions that allowed us to analyze how multiple LNP chemical variables interacted with one another. This future work is important, given that changing 1 LNP parameter often impacts another (e.g., adding more PEG to the LNP concomitantly reduces cholesterol).

Nanoparticle biodistribution is quantified using ex vivo tissue fluorescence; however, it is still unclear how different cell types within a tissue microenvironment are targeted.[5,16] More specifically, it is unclear which cell types tend to be targeted by similar LNPs. To address this question, we focused on the spleen; LNPs can deliver nucleic acids to[38] and be cleared by[16] the spleen. We formulated a fourth LNP library. Library 4 consisted of 144 LNPs, of which 85 were found to be stable by DLS, and included (Figure S5a,b). We administered library 4 to RAWs and mice and isolated eight different cell types using FACS (Figure 5a, Figure S5c). We performed unbiased Euclidean clustering, which is used to simultaneously compare how many experimental groups relate to one another (Figure 5b). This technique is commonly used in bioinformatics to "cluster" samples that share more similarity to one another than with other samples. Euclidean clustering recapitulated our results from libraries 1−3, separating in vivo delivery to all cell types (including macrophages) from in vitro delivery to RAWs (Figure 5b,c,g).

Interestingly, the seven immune cell subtypes clustered into cells derived from myeloid progenitors and lymphoid progenitors. Plasmacytoid and conventional dendritic cells were clustered most closely with one another, and also clustered closely with macrophages and neutrophils (Figure 5b,c). All four cell types derive from a common progenitor. T cells, B cells, and natural killer cells, which derive from a different progenitor, clustered together (Figure 5b,c). This suggests that nanoparticles which targeted one cell type derived from myeloid progenitors were more likely to target another cell type derived from myeloid progenitors, compared to a cell type derived from a lymphoid progenitor. To quantify this clustering, we measured the correlation between all tested cell types (Figure 5c). Conventional DCs and plasmacytoid DCs, which clustered together, were highly correlated to each other (R^2 = 0.90) (Figure 5c,d), as were B cells and T cells (R^2 = 0.88) (Figure 5c,e). Cells derived from myeloid progenitors (e.g., conventional DCs) and lymphoid progenitors (e.g., T cells) had a much weaker correlation (R^2 = 0.2) (Figure 5f).

DOI: 10.1021/acs.nanolett.8b00432
Nano Lett. XXXX, XXX, XXX−XXX

These data demonstrate a unique capability for the JORDAN system; directly comparing how dozens of LNPs deliver nucleic to seven different cell types would be very challenging using traditional one-by-one methods (e.g., fluorescence).

Using delivery data generated from this screen, we identified two LNPs for additional characterization (Figure 6a). Barcodes delivered by LNP1 were enriched in all eight splenic cell types, relative to barcodes delivered by LNP2 (Figure 6b,c). We formulated LNP1 and LNP2 separately, using a Cy5.5-tagged DNA barcode, and injected mice intravenously with 0.75 mg/kg DNA barcode. LNP1-treated mice had 12.1 times more splenic Cy5.5 ex vivo fluorescence than LNP2-treated mice, recapitulating the barcode readouts (Figure 6d).

Discussion. We found that in vivo delivery to macrophages and endothelial cells is not predicted in vitro using common cell culture conditions. Modeling all the factors (e.g., blood flow, vascular heterogeneity, systemic, and local immune cells, unwanted delivery to clearance organs) that influence nanoparticles in vivo is challenging. These results have important implications for nanoparticle design, given that nanoparticles are typically selected in vitro. We initially compared delivery to five different cell lines and six different in vivo cell types; it will be important to determine whether these results extend to other cell types and cell culture conditions. For example, it was previously shown that delivery in primary hepatocytes was more predictive of in vivo delivery than a hepatoma cell line.[39] At first glance, our results may seem to contradict this work. We believe they do not; both studies underscore the importance of characterizing how well a given in vitro system predicts a desired in vivo outcome. To this end, we believe JORDAN is well positioned to optimize organ-on-a-chip[40] and organoids[41] designed to predict in vivo behavior by acting as a positive control.

JORDAN is agnostic to cell type and animal model. This allowed us to easily study drug delivery to eight different splenic cell types in a single experiment. Testing how many LNPs target several cell types may lead to interesting discoveries. For example, our results suggest cells derived from myeloid progenitors tend to be targeted by the similar LNPs. This provides preliminary evidence that gene expression patterns that promote LNP delivery to phagocytic cells may be identified. However, these results need to be validated using other nanoparticles.

We noticed that there were practical advantages to using the JORDAN system. Testing many nanoparticles at once reduces experimental variation that occurs when experiments performed over months are compared to one another. We previously screened LNPs one by one;[5] it was difficult to ensure kits, reagents, and cell passage number were perfectly consistent. By testing many LNPs on the same day, it is easier to reduce unintentional experimental bias. At the same time, the JORDAN system has limitations. JORDAN is unlikely to work with unstable or toxic LNPs; it is critical to characterize particles before pooling them. JORDAN measures biodistribution, which is required, but not sufficient, for intracellular delivery. It will also be important to prevent PCR contamination. Finally, like all high throughput screening systems, lead candidates need to be independently verified. For example, we identified LNP1, which performed well in our barcode screen, and LNP2, which performed poorly in our barcode screen, before confirming their activity one by one (Figures 5 and 6). As part of our original barcoding study,[18] we performed a similar confirmation experiment using Factor 7 siRNA.

Despite these caveats, our data demonstrate that JORDAN is a powerful new tool to help researchers understand in vivo drug delivery. We also believe the differences between in vitro and in vivo delivery suggest that in vivo screening may accelerate the rate at which clinically relevant LNPs can be discovered. To help other laboratories use the JORDAN system, we have published an open-source, "living" document, which details reagents, protocols and our LNP bioinformatics pipeline on dahlmanlab.org.

Materials and Methods. *Nanoparticle Formulation.* Nanoparticles were formulated in a microfluidic device by mixing DNA with lipomer, PEG, cholesterol, and a helper lipid, as previously described.[5,18,19,22−27,42] Nanoparticles were made with variable mole ratios of these constituents. The genetic drug (in this case, DNA barcode) was diluted in 10 mM citrate buffer (Teknova), and loaded into a syringe (Hamilton Company). The materials making up the nanoparticle (lipomer, cholesterol, PEG, and helper lipid) were diluted in 100% ethanol and loaded into a second syringe. The citrate phase and ethanol phase were mixed together in a microfluidic device, at rates of 600 uL/min and 200 uL/min, respectively, to form LNPs. We used the following helper lipids: DOPE (Avanti Lipids, 850725), and DOPC (Avanti Lipids, 850375).

DNA barcoding. Each chemically distinct LNP was formulated to carry its own unique DNA barcode (Figure 1a,b). For example, LNP1 carried DNA barcode 1, while the chemically distinct LNP2 carried DNA barcode 2.

The DNA barcodes were designed rationally with several characteristics, as we previously described.[18] We purchased 56 nucleotide single-stranded DNA sequences from IDT (Figure 1c, Figure S1a). We included 2 universal 21 and 20 nucleotide primer regions in addition to a random 7 nucleotide ("7N") region that is unique to each piece of DNA (Figure S1b). Barcodes were distinguished using an eight basepair (bp) sequence in the middle of the barcode. An 8 bp sequence can generate over 65,000 (4^8) unique barcodes; we selected 240 barcodes to prevent sequence bleaching on the Illumina MiniSeq machine. The two nucleotides on the 5′ and 3′ ends of the 56-nucleotide ssDNA sequence were modified with phosphorothioate linkages to reduce exonuclease degradation and improve DNA barcode stability.

Nanoparticle Characterization. LNP hydrodynamic diameter was measured using high throughput dynamic light scattering (DLS) (DynaPro Plate Reader II, Wyatt). LNPs were diluted in sterile 1× PBS to a concentration of ∼0.0005 mg/mL, and analyzed. LNPs were included if they met three criteria: diameter >20 nm, diameter <300 nm, and autocorrelation function with only one inflection point. Over the course of our experiments, ∼65% of the LNPs we formulated met all three criteria. Particles that met these criteria were pooled and dialyzed with 1× phosphate buffered saline (PBS, Invitrogen) and were sterile filtered with a 0.22 μm filter.

Animal Experiments. All animal experiments were performed in accordance with the Georgia Institute of Technology's Institutional Animal Care and Use Committee (IACUC). Female C57BL/6J (#000664) mice were purchased from the Jackson Laboratory. All mouse weights before and after injection are shown in (Figure S6a,b). In all experiments, mice were aged 4−12 weeks, female, and N = 3−5 mice per

DOI: 10.1021/acs.nanolett.8b00432
Nano Lett. XXXX, XXX, XXX−XXX

group were injected intravenously via the lateral tail vein with the same pooled LNPs.

Nanoparticle Dosing. Mice were injected with a total DNA dose of 0.5 mg/kg. As an example, if an experiment measured 100 nanoparticles then on average each nanoparticle was administered at a dose of 0.005 mg/kg. The nanoparticle dose was determined using NanoDrop (Thermo Scientific).

Cell Culture. In vitro experiments were performed using mouse macrophage cells (RAW 264.7, ATCC), mouse aortic endothelial cells (provided by Hanjoong Jo at Emory),[34] primary human aortic endothelial cells (HAEC, Lonza), primary human umbilical vein endothelial cells (HUVEC, Lonza), and primary human aortic vein endothelial cells (HAVEC, Lonza).

In all cases, cells were maintained and cultured using previously established conditions. In all cases, cell media was supplemented by penicillin−streptomycin (500 U/mL penicillin G, 0.5 mg/mL streptomycin) (PenStrep, VWR) and 10% (v/v) fetal bovine serum (FBS, VWR). RAW cells were passaged with DMEM F-12 50/50 (Corning). iMAEC cells were passaged using DMEM with 1 g/L glucose, L-glutamine, and sodium pyruvate (Corning), supplemented by 1% (v/v) MEM nonessential amino acid solution (MEMNEAA, Sigma-Aldrich), and 25 μg/mL endothelial cell growth supplement (ECGS, Emd Millipore). HAEC and HAVEC cells were passaged with MCDB 131 media without L-glutamine (VWR Scientific), supplemented by 1% (v/v) L-glutamate, 25 μg/mL ECGS, 0.1% (v/v) ascorbic acid, hydrocortisol, and the following growth factors: endothelial growth factor (EGF), vascular-endothelial growth factor (VEGF), fibroblast growth factor (FGF), and insulin-like growth factor (IGF). HUVEC cells were passaged with M199 media with Earle's salts and L-glutamine (Corning), supplemented by 1% (v/v) ECGS, L-glutamine, and 0.2% (v/v) heparin.

In all cases, cells were seeded in a 24-well plate at a density of 40,000 cells/well. Twenty-four hours later, LNPs were added with a total DNA dose of 4, 20, or 100 ng (Figure 2e, Figure S2b−d). On the basis of these results, cells were treated with 20 ng total DNA in all other experiments. Six hours after transfection, media was removed, and fresh media was added. Seventy-two hours after transfection, media was removed and DNA was isolated using QuickExtract (EpiCentre).

Fixed-Cell Staining. Cells were plated onto 35 mm glass-bottom dishes (In Vitro Scientific) 1 day prior to particle delivery. Cells were fixed at the indicated time points with 4% paraformaldehyde (Electron Microscopy Sciences) for 10 min at room temperature before permeabilization with 0.2% Triton X-100 (Sigma-Aldrich) for 5 min at room temperature. To stain actin, cells were then incubated with Phalloidin-488 (Thermo Scientific) for 30 min at 37 °C. Nuclei were stained with 4′,6-diamidino-2-phenylindole (DAPI) (Life Technologies), and coverslips were placed over the cells in the dish and mounted with Prolong Gold (Life Technologies).

Microscopy. Images were acquired with a Hamamatsu Flash 4.0 v2 sCMOS camera on a PerkinElmer UltraView spinning disk confocal microscope mounted to a Zeiss Axiovert 200 M body with a 63× NA 1.4 plan-apochromat objective. Images were acquired with Volocity (PerkinElmer) with Z-stacks taken in 0.2 μm increments. For live-cell images, cells and dishes were kept at 37 °C during imaging by using a Chamlide TC-L live-cell stage-top environment with objective heater (Live Cell Instrument). All images were linearly contrast enhanced. Live-cell images were smoothed with a fine rolling ball filter in Volocity.

Cell Isolation. One time-course experiment was performed; delivery was analyzed 4, 48, and 72 h after LNPs were administered. In all other cases, tissues and cells were isolated 72 h after injection with LNPs. In all experiments, mice were perfused with 20 mL of 1× PBS through the right atrium. The heart, lungs, spleen, and bone marrow were isolated immediately following perfusion. Tissues were finely cut and then placed in a digestive enzyme solution with Collagenase Type I (Sigma-Aldrich), Collagenase XI (Sigma-Aldrich), and Hyaluronidase (Sigma-Aldrich). The digestive enzyme for heart included Collagenase IV (Sigma-Aldrich).[22] Tissues were digested for 45 min at 37 °C and 550 rpm. Digested tissues were passed through a 70 μm filter. Red blood cells were lysed using (RBC) lysis buffer. Cells were resuspended in FACS buffer (2% FBS in 1× PBS).

Heart, Lung, and Bone Marrow Cell Staining. Cells were stained to identify specific cell populations and sorted using the BD FacsFusion and BD Facs Aria IIIu cell sorters in the Georgia Institute of Technology cellular analysis core. Antibodies used for staining were CD31 (clone 390, BioLegend), CD45.2 (clone 104, BioLegend), and CD11b (clone M1/70, BioLegend).

We defined cell populations in the following manner: macrophages ($CD31^{-}CD45^{+}CD11b^{+}$), heart and lung endothelial cells ($CD31^{+}CD45^{-}$), and bone marrow endothelial cells ($CD31^{+}$) (S3A-C).

Splenic Cell Staining and Isolation. Splenocytes were isolated by digesting sliced spleens in 0.1 U/mL collagenase (Sigma-Aldrich) in Hank's Balanced Salt Solution (Corning) for 30 min at 37 °C. Digestion was stopped by addition of EDTA to 5 mM, and the resulting mixture was passed through a cell strainer. Red blood cells were removed with ACK lysing buffer (Lonza), and cells were washed in FACS buffer (PBS supplemented with 2% FBS and 2 mM EDTA; Corning and HyClone) and restrained.

Cells were stained by conventional methods in FACS buffer as previously described.[43] Antibodies used for staining were CD19 (clone 1D3, eBioscience), CD3 (clone 17A2, eBioscience), CD31 (clone 390, BioLegend), CD45 (clone 104, BioLegend), NK1.1 (clone PK136, eBioscience), CD11b (clone M1/70, BioLegend), CD11c (clone N418, BioLegend), Siglec H (clone 551, BioLegend), F4/80 (clone BM8, BioLegend), and Ly-6G (clone 1A8, BioLegend). Cells were also stained with LIVE/DEAD viability dyes (Thermo Fisher) to exclude dead cells.

Described splenocyte cell types (Figure 5a, Figure S5c) from four mice were isolated by FACS on two FACSAria II cell sorters (BD Biosciences) at the Emory University School of Medicine Flow Cytometry Core.

PCR Amplification. All samples were amplified and prepared for sequencing. More specifically, 1 μL of primers (5 μM for Final Reverse/Forward, 0.5 μM for Base Forward) were added to 5 μL of Kapa HiFi 2× master mix, 3 μL of sterile H_2O, and 1 μL of DNA template. The reaction was run for 30 cycles. When the PCR reaction did not produce clear bands, the primer concentrations, DNA template input, PCR temperature, and number of cycles were optimized for individual samples. The PCR amplicon was isolated with gel extraction.

Deep Sequencing. Illumina deep sequencing was conducted in Georgia Tech's Molecular Evolution core. Runs were

DOI: 10.1021/acs.nanolett.8b00432
Nano Lett. XXXX, XXX, XXX−XXX

performed on an Illumina Miniseq Primers were designed based on Nextera XT adapter sequences.

Data Normalization. Counts for each particle, per tissue, were normalized to unity (Figure 1d) The DNA counts in each tissue were then normalized to 100%. For example, if a sample (e.g., heart1) had 500,000 total barcode reads, and 50,000 of them came from particle X, while 4,000 came from particle Y, then the normalized delivery for particle X and Y would be 10% and 0.8%, respectively. The barcoded LNP mixture we injected into the mouse was also sequenced. This "input" DNA was used to normalize DNA counts from the cells and tissues (Figure S1c).

Data Analysis. Sequencing results were processed using a custom python-based tool to extract raw barcode counts for each tissue. These raw counts were then normalized with an *R* script prior to further analysis. Statistical analysis was done using GraphPad Prism 7. Correlation analyses were run assuming a Gaussian distribution in order to obtain Pearson correlation coefficients. R^2 values (0−1) were computed by squaring Pearson correlation coefficients.

■ ASSOCIATED CONTENT

Supporting Information

The Supporting Information is available free of charge on the ACS Publications website at DOI: 10.1021/acs.nanolett.8b00432.

Barcode sequences used, NGS primers, normalization procedure, in vitro barcode imaging; library 1 design, in vitro dose response; FACs gating strategies for endothelial cells and macrophages, library 2 and 3 design, LNP diameter distributions, in vitro versus in vivo and primary cell data set complementing Figure 2; macrophage data set complementing Figure 4a,b, in vivo endothelial cells and macrophages plotted according to in vitro rank, LNP structures and Supporting Information for ranked particles in endothelial cells and macrophages, significant and nonsignificant relationships between LNP structure and cell targeting; LNP library used for spleen biodistribution, FACs gating strategy for spleen; mouse weights for all experiments relative to control (PBS) (PDF)

■ AUTHOR INFORMATION

Corresponding Author

*E-mail: james.dahlman@bme.gatech.edu.

ORCID

James E. Dahlman: 0000-0001-7580-436X

Author Contributions

⊥K.P. and C.D.S. contributed equally to this work. K.P., C.D.S., and J.E.D. designed experiments. All authors performed the experiments and/or analyzed the data. K.P., C.D.S., and J.E.D. wrote the paper with input from all authors.

Funding

C.D.S., K.P., and J.E.D. were funded by Georgia Tech startup funds (awarded to J.E.D.). C.M.M. was funded by the Georgia Research Assistantship (Grant 3201330). K.P. was also funded by the NIH/NIGMS-sponsored Cell and Tissue Engineering (CTEng) Biotechnology Training Program (T32GM008433). C.D.S. was also funded by the NIH/NIGMS-sponsored Immunoengineering Training Program (T32EB021962). W.H.H is a Cancer Research Institute Irvington Fellow supported by the Cancer Research Institute. Research was funded by the Cystic Fibrosis Research Foundation (DAHLMA15XX0, awarded to J.E.D.), the Parkinson's Disease Foundation (PDF-JFA-1860, awarded to J.E.D.), and the Bayer Hemophilia Awards Program (AGE DTD, awarded to J.E.D.). This study was also supported with funding from the National Institutes of Health GT BioMAT Training Grant under Award Number (5T32EB006343). This work was performed in part at the Georgia Tech Institute for Electronics and Nanotechnology, a member of the National Nanotechnology Coordinated Infrastructure, which is supported by the National Science Foundation (Grant ECCS-1542174).

Notes

The authors declare no competing financial interest.

The data, analyses, and scripts used to generate all figures in the paper are available upon request to J.E.D. or dahlmanlab.org.

■ ACKNOWLEDGMENTS

The authors thank Jordan Cattie, Gabriel Kwong, Melissa Kemp, Marwa Mahmoud, Hanjoong Jo, and Timothy Mark O'Shea for providing helpful feedback as well as cells and reagents. The authors thank Sommer Durham and the Georgia Tech Cellular Analysis and Cytometry Core. The authors thank Robert Karaffa, Conner Carter, and the Emory University School of Medicine Flow Cytometry Core. Finally, J.E.D. thanks Taylor E. Shaw.

■ REFERENCES

(1) Blanco, E.; Shen, H.; Ferrari, M. *Nat. Biotechnol.* **2015**, *33* (9), 941−51.

(2) Cheng, C. J.; Tietjen, G. T.; Saucier-Sawyer, J. K.; Saltzman, W. M. *Nat. Rev. Drug Discovery* **2015**, *14* (4), 239−47.

(3) Sahin, U.; Kariko, K.; Tureci, O. *Nat. Rev. Drug Discovery* **2014**, *13* (10), 759−80.

(4) Dong, Y.; Love, K. T.; Dorkin, J. R.; Sirirungruang, S.; Zhang, Y.; Chen, D.; Bogorad, R. L.; Yin, H.; Chen, Y.; Vegas, A. J.; Alabi, C. A.; Sahay, G.; Olejnik, K. T.; Wang, W.; Schroeder, A.; Lytton-Jean, A. K.; Siegwart, D. J.; Akinc, A.; Barnes, C.; Barros, S. A.; Carioto, M.; Fitzgerald, K.; Hettinger, J.; Kumar, V.; Novobrantseva, T. I.; Qin, J.; Querbes, W.; Koteliansky, V.; Langer, R.; Anderson, D. G. *Proc. Natl. Acad. Sci. U. S. A.* **2014**, *111* (11), 3955−60.

(5) Dahlman, J. E.; Barnes, C.; Khan, O. F.; Thiriot, A.; Jhunjunwala, S.; Shaw, T. E.; Xing, Y.; Sager, H. B.; Sahay, G.; Speciner, L.; Bader, A.; Bogorad, R. L.; Yin, H.; Racie, T.; Dong, Y.; Jiang, S.; Seedorf, D.; Dave, A.; Singh Sandhu, K.; Webber, M. J.; Novobrantseva, T.; Ruda, V. M.; Lytton-JeanAbigail, K. R.; Levins, C. G.; Kalish, B.; Mudge, D. K.; Perez, M.; Abezgauz, L.; Dutta, P.; Smith, L.; Charisse, K.; Kieran, M. W.; Fitzgerald, K.; Nahrendorf, M.; Danino, D.; Tuder, R. M.; von Andrian, U. H.; Akinc, A.; Panigrahy, D.; Schroeder, A.; Koteliansky, V.; Langer, R.; Anderson, D. G. *Nat. Nanotechnol.* **2014**, *9* (8), 648−655.

(6) Love, K. T.; Mahon, K. P.; Levins, C. G.; Whitehead, K. A.; Querbes, W.; Dorkin, J. R.; Qin, J.; Cantley, W.; Qin, L. L.; Racie, T.; Frank-Kamenetsky, M.; Yip, K. N.; Alvarez, R.; Sah, D. W.; de Fougerolles, A.; Fitzgerald, K.; Koteliansky, V.; Akinc, A.; Langer, R.; Anderson, D. G. *Proc. Natl. Acad. Sci. U. S. A.* **2010**, *107* (5), 1864−9.

(7) Akinc, A.; Zumbuehl, A.; Goldberg, M.; Leshchiner, E. S.; Busini, V.; Hossain, N.; Bacallado, S. A.; Nguyen, D. N.; Fuller, J.; Alvarez, R.; Borodovsky, A.; Borland, T.; Constien, R.; de Fougerolles, A.; Dorkin, J. R.; Narayanannair Jayaprakash, K.; Jayaraman, M.; John, M.; Koteliansky, V.; Manoharan, M.; Nechev, L.; Qin, J.; Racie, T.; Raitcheva, D.; Rajeev, K. G.; Sah, D. W.; Soutschek, J.; Toudjarska, I.; Vornlocher, H. P.; Zimmermann, T. S.; Langer, R.; Anderson, D. G. *Nat. Biotechnol.* **2008**, *26* (5), 561−9.

DOI: 10.1021/acs.nanolett.8b00432
Nano Lett. XXXX, XXX, XXX−XXX

(8) Hao, J.; Kos, P.; Zhou, K.; Miller, J. B.; Xue, L.; Yan, Y.; Xiong, H.; Elkassih, S.; Siegwart, D. J. *J. Am. Chem. Soc.* **2015**, *137* (29), 9206−9209.
(9) Siegwart, D. J.; Whitehead, K. A.; Nuhn, L.; Sahay, G.; Cheng, H.; Jiang, S.; Ma, M.; Lytton-Jean, A.; Vegas, A.; Fenton, P.; Levins, C. G.; Love, K. T.; Lee, H.; Cortez, C.; Collins, S. P.; Li, Y. F.; Jang, J.; Querbes, W.; Zurenko, C.; Novobrantseva, T.; Langer, R.; Anderson, D. G. *Proc. Natl. Acad. Sci. U. S. A.* **2011**, *108* (32), 12996−3001.
(10) Zuckerman, J. E.; Choi, C. H.; Han, H.; Davis, M. E. *Proc. Natl. Acad. Sci. U. S. A.* **2012**, *109* (8), 3137−42.
(11) Aird, W. C. *Crit. Care Med.* **2003**, *31* (4), S221−S230.
(12) Aird, W. C. *Cold Spring Harbor Perspect. Med.* **2012**, *2* (1), a006429.
(13) Aird, W. C. *Circ. Res.* **2007**, *100* (2), 174−190.
(14) Aird, W. C. *Circ. Res.* **2007**, *100* (2), 174−190.
(15) Augustin, H. G.; Koh, G. Y. *Science* **2017**, *357* (6353), No. eaal2379.
(16) Tsoi, K. M.; MacParland, S. A.; Ma, X. Z.; Spetzler, V. N.; Echeverri, J.; Ouyang, B.; Fadel, S. M.; Sykes, E. A.; Goldaracena, N.; Kaths, J. M.; Conneely, J. B.; Alman, B. A.; Selzner, M.; Ostrowski, M. A.; Adeyi, O. A.; Zilman, A.; McGilvray, I. D.; Chan, W. C. *Nat. Mater.* **2016**, *15* (11), 1212−1221.
(17) Zhang, Y.; Sloan, S. A.; Clarke, L. E.; Caneda, C.; Plaza, C. A.; Blumenthal, P. D.; Vogel, H.; Steinberg, G. K.; Edwards, M. S.; Li, G.; Duncan, J. A., 3rd; Cheshier, S. H.; Shuer, L. M.; Chang, E. F.; Grant, G. A.; Gephart, M. G.; Barres, B. A. *Neuron* **2016**, *89* (1), 37−53.
(18) Dahlman, J. E.; Kauffman, K. J.; Xing, Y.; Shaw, T. E.; Mir, F. F.; Dlott, C. C.; Langer, R.; Anderson, D. G.; Wang, E. T. *Proc. Natl. Acad. Sci. U. S. A.* **2017**, *114* (8), 2060−2065.
(19) Chen, D.; Love, K. T.; Chen, Y.; Eltoukhy, A. A.; Kastrup, C.; Sahay, G.; Jeon, A.; Dong, Y.; Whitehead, K. A.; Anderson, D. G. *J. Am. Chem. Soc.* **2012**, *134* (16), 6948−51.
(20) Carmeliet, P.; Jain, R. K. *Nature* **2011**, *473* (7347), 298−307.
(21) Swirski, F. K.; Nahrendorf, M. *Science* **2013**, *339* (6116), 161−6.
(22) Sager, H. B.; Dutta, P.; Dahlman, J. E.; Hulsmans, M.; Courties, G.; Sun, Y.; Heidt, T.; Vinegoni, C.; Borodovsky, A.; Fitzgerald, K.; Wojtkiewicz, G. R.; Iwamoto, Y.; Tricot, B.; Khan, O. F.; Kauffman, K. J.; Xing, Y.; Shaw, T. E.; Libby, P.; Langer, R.; Weissleder, R.; Swirski, F. K.; Anderson, D. G.; Nahrendorf, M. *Sci. Transl. Med.* **2016**, *8* (342), 342ra80−342ra80.
(23) Yun, S.; Budatha, M.; Dahlman, J. E.; Coon, B. G.; Cameron, R. T.; Langer, R.; Anderson, D. G.; Baillie, G.; Schwartz, M. A. *Nat. Cell Biol.* **2016**, *18*, 1043.
(24) Xue, W.; Dahlman, J. E.; Tammela, T.; Khan, O. F.; Sood, S.; Dave, A.; Cai, W.; Chirino, L. M.; Yang, G. R.; Bronson, R.; Crowley, D. G.; Sahay, G.; Schroeder, A.; Langer, R.; Anderson, D. G.; Jacks, T. *Proc. Natl. Acad. Sci. U. S. A.* **2014**, *111* (34), E3553−E3561.
(25) Platt, R. J.; Chen, S.; Zhou, Y.; Yim, M. J.; Swiech, L.; Kempton, H. R.; Dahlman, J. E.; Parnas, O.; Eisenhaure, T. M.; Jovanovic, M.; Graham, D. B.; Jhunjhunwala, S.; Heidenreich, M.; Xavier, R. J.; Langer, R.; Anderson, D. G.; Hacohen, N.; Regev, A.; Feng, G.; Sharp, P. A.; Zhang, F. *Cell* **2014**, *159* (2), 440−55.
(26) Sager, H. B.; Hulsmans, M.; Lavine, K. J.; Moreira, M. B.; Heidt, T.; Courties, G.; Sun, Y.; Iwamoto, Y.; Tricot, B.; Khan, O. F.; Dahlman, J. E.; Borodovsky, A.; Fitzgerald, K.; Anderson, D. G.; Weissleder, R.; Libby, P.; Swirski, F. K.; Nahrendorf, M. *Circ. Res.* **2016**, *119* (7), 853−64.
(27) White, K.; Lu, Y.; Annis, S.; Hale, A. E.; Chau, B. N.; Dahlman, J. E.; Hemann, C.; Opotowsky, A. R.; Vargas, S. O.; Rosas, I.; Perrella, M. A.; Osorio, J. C.; Haley, K. J.; Graham, B. B.; Kumar, R.; Saggar, R.; Saggar, R.; Wallace, W. D.; Ross, D. J.; Khan, O. F.; Bader, A.; Gochuico, B. R.; Matar, M.; Polach, K.; Johannessen, N. M.; Prosser, H. M.; Anderson, D. G.; Langer, R.; Zweier, J. L.; Bindoff, L. A.; Systrom, D.; Waxman, A. B.; Jin, R. C.; Chan, S. Y. *EMBO Mol. Med.* **2015**, *7* (6), 695−713.
(28) Khan, O. F.; Zaia, E. W.; Jhunjhunwala, S.; Xue, W.; Cai, W.; Yun, D. S.; Barnes, C. M.; Dahlman, J. E.; Dong, Y.; Pelet, J. M.; Webber, M. J.; Tsosie, J. K.; Jacks, T. E.; Langer, R.; Anderson, D. G. *Nano Lett.* **2015**, *15* (5), 3008−16.
(29) Khan, O. F.; Zaia, E. W.; Yin, H.; Bogorad, R. L.; Pelet, J. M.; Webber, M. J.; Zhuang, I.; Dahlman, J. E.; Langer, R.; Anderson, D. G. *Angew. Chem., Int. Ed.* **2014**, *53* (52), 14397−401.
(30) Wittrup, A.; Ai, A.; Liu, X.; Hamar, P.; Trifonova, R.; Charisse, K.; Manoharan, M.; Kirchhausen, T.; Lieberman, J. *Nat. Biotechnol.* **2015**, *33*, 870.
(31) Gilleron, J.; Querbes, W.; Zeigerer, A.; Borodovsky, A.; Marsico, G.; Schubert, U.; Manygoats, K.; Seifert, S.; Andree, C.; Stoter, M.; Epstein-Barash, H.; Zhang, L.; Koteliansky, V.; Fitzgerald, K.; Fava, E.; Bickle, M.; Kalaidzidis, Y.; Akinc, A.; Maier, M.; Zerial, M. *Nat. Biotechnol.* **2013**, *31* (7), 638−46.
(32) Geary, R. S.; Norris, D.; Yu, R.; Bennett, C. F. *Adv. Drug Delivery Rev.* **2015**, *87*, 46−51.
(33) Crooke, S. T.; Wang, S.; Vickers, T. A.; Shen, W.; Liang, X. H. *Nat. Biotechnol.* **2017**, *35* (3), 230−237.
(34) Ni, C. W.; Kumar, S.; Ankeny, C. J.; Jo, H. *Vasc. Cell* **2014**, *6* (1), 7.
(35) Kumar, V.; Qin, J.; Jiang, Y.; Duncan, R. G.; Brigham, B.; Fishman, S.; Nair, J. K.; Akinc, A.; Barros, S. A.; Kasperkovitz, P. V. *Mol. Ther.–Nucleic Acids* **2014**, *3*, e210.
(36) Tao, W.; Davide, J. P.; Cai, M.; Zhang, G. J.; South, V. J.; Matter, A.; Ng, B.; Zhang, Y.; Sepp-Lorenzino, L. *Mol. Ther.* **2010**, *18* (9), 1657−66.
(37) Mui, B. L.; Tam, Y. K.; Jayaraman, M.; Ansell, S. M.; Du, X.; Tam, Y. Y.; Lin, P. J.; Chen, S.; Narayanannair, J. K.; Rajeev, K. G.; Manoharan, M.; Akinc, A.; Maier, M. A.; Cullis, P.; Madden, T. D.; Hope, M. J. *Mol. Ther.–Nucleic Acids* **2013**, *2*, e139.
(38) Kranz, L. M.; Diken, M.; Haas, H.; Kreiter, S.; Loquai, C.; Reuter, K. C.; Meng, M.; Fritz, D.; Vascotto, F.; Hefesha, H.; Grunwitz, C.; Vormehr, M.; Husemann, Y.; Selmi, A.; Kuhn, A. N.; Buck, J.; Derhovanessian, E.; Rae, R.; Attig, S.; Diekmann, J.; Jabulowsky, R. A.; Heesch, S.; Hassel, J.; Langguth, P.; Grabbe, S.; Huber, C.; Tureci, O.; Sahin, U. *Nature* **2016**, *534* (7607), 396−401.
(39) Whitehead, K. A.; Matthews, J.; Chang, P. H.; Niroui, F.; Dorkin, J. R.; Severgnini, M.; Anderson, D. G. *ACS Nano* **2012**, *6* (8), 6922−9.
(40) Bhatia, S. N.; Ingber, D. E. *Nat. Biotechnol.* **2014**, *32* (8), 760−72.
(41) Fatehullah, A.; Tan, S. H.; Barker, N. *Nat. Cell Biol.* **2016**, *18* (3), 246−254.
(42) Koga, J.; Nakano, T.; Dahlman, J. E.; Figueiredo, J. L.; Zhang, H.; Decano, J.; Khan, O. F.; Niida, T.; Iwata, H.; Aster, J. C.; Yagita, H.; Anderson, D. G.; Ozaki, C. K.; Aikawa, M. *Arterioscler., Thromb., Vasc. Biol.* **2015**, *35* (11), 2343−53.
(43) Araki, K.; Morita, M.; Bederman, A. G.; Konieczny, B. T.; Kissick, H. T.; Sonenberg, N.; Ahmed, R. *Nat. Immunol.* **2017**, *18* (9), 1046−1057.

DOI: 10.1021/acs.nanolett.8b00432
Nano Lett. XXXX, XXX, XXX−XXX